Lasers in Manufacturing Conference 2023

Influence of laser beam welding in vacuum on the residual stress of non-grain oriented electrical steel sheets

Thomas Krichel[a,*], Simon Olschok[a], Uwe Reisgen[a]

[a]*Welding and Joining Institute RWTH Aachen University, Pontstr. 49, 52062 Aachen, Germany*

Abstract

Major components of electrical motors are iron cores made of stacked electrical steel sheets to reduce eddy current loss. All common joining methods cause a degradation of the magnetic properties of the iron cores. Using fusion welding methods thermally induced residual stress degrade the magnetic properties. In this paper, pulsed laser beam welding in vacuum is used to join the individual electrical steel sheets. It is shown, that the intensity of residual stress can be influenced by variation of process parameters like beam power and working pressure.

Keywords: electrical steel sheets; laser beam welding in vacuum; residual stress

1. Introduction

Modern electric motors are indispensable components in almost all industrial processes and most areas of daily life. Their use in fully or partially electrically driven vehicles, for example, offers advantages over the classic combustion engine. The efficiency of electric motors depends on the speed of the rotor, the re-magnetisation frequency f_{UM} at which the magnetic field is reversed, and the torque to be transmitted. In the automotive sector, a re-magnetisation frequency of e.g. f_{UM} = 1000 Hz is frequently used, whereby efficiencies of 60 % to 94 % are achieved [1, 2]. In comparison, conventional diesel and petrol combustion engines currently only achieve efficiencies of up to 50 % [3, 4]. In addition, the electric motor is very low in

* *Corresponding author. Tel.: +49 241 80-96323*
E-mail address: krichel@isf.rwth-aachen.de

emissions during operation in terms of noise and climate-damaging gases and offers mobility independent of finite, non-renewable resources [5, 6].

The basic elements of any electric motor are a rigid component (stator) and a rotating component (rotor). Both components contain a ring-shaped core wrapped with copper wire. To convert electrical energy into mechanical energy, a magnetic field is generated in the stator by applying an electrical voltage, which causes the rotor to rotate by repeatedly reversing the polarity or magnetisation [6].

The toroidal cores are constructed from many layers of sheet metal electrically insulated from each other in order to increase the inductance of the toroidal cores and reduce eddy current losses [6, 7]. In the case of the material specially produced for this purpose, the "electrical steel sheet", a distinction is made between grain-oriented electrical sheet, which is used e.g. in transformers, and non-grain-oriented electrical sheet, which is preferred for electric motors due to its isotropic magnetic properties [8-10].

Any packaging process, e.g. permanently joining a stack of sheets to a toroidal core, degrades the magnetic properties compared to the unbonded stack of sheets, e.g. due to geometric changes or the creation of short-circuit paths. Various methods are used to join the stack of sheets, including welding, punching, riveting and gluing [11-13].

In addition to welding defects such as pores or spatter, not least residual stresses also have a negative influence on the magnetic properties, since both the energy required to generate and maintain the rotary motion and the dissipation increase [14, 15].

When stacking with a laser beam welding process, the stack of laminations is usually joined by line welds along the axis of rotation on the outer radius of the toroidal core, Figure 1, left. The heat input during welding leads to changes in the grain structure and residual stresses, especially longitudinal tensile stresses along the weld, which have a negative effect on the magnetic properties of the toroidal cores [11, 16-20]. As an alternative to line welding, pulsed laser beam welding is used here to apply individual, statistically equally distributed weld spots to the core's shell, Figure 1, right. This reduces the local energy input and creates a hemispherical seam geometry.

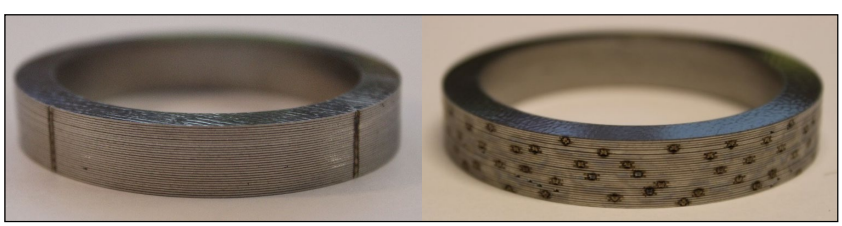

Fig. 1. Different joining strategies of t toroidal cores, Left: Line welds, Right: statistically distributed spot welds

The quantification of residual stresses in solid materials cannot be done by direct measurements, but only by calculations. An established method for determining residual stresses is the incremental borehole method, which was described as early as 1933 by Josef Mathar and is now regulated in ASTM E837-08 [21]. In this method, a hole is milled step-by-step into a specimen surface that has been subjected to low stress, causing the residual stress conditions in the material to change. With each depth increment by which the hole becomes deeper, plastic deformations occur at the surface of the specimen due to the release of residual stresses at the edge of the hole and in its immediate vicinity. These geometric changes are classically recorded with strain gauges, which, however, can only cover part of the surrounding area of the borehole. In order to detect the entire deformations and increase the measurement accuracy, optical measurement methods such as electronic speckle pattern interferometry (ESPI) are used [22-27].

With the help of ESPI, the total geometry changes of the sample surface that occur during the insertion of the blind hole become quantifiable. For this purpose, the hole and its immediate surroundings are illuminated with laser light, which is reflected depending on the angle of incidence and the surface roughness of the sample and generates the so-called speckle patten, Figure 2.

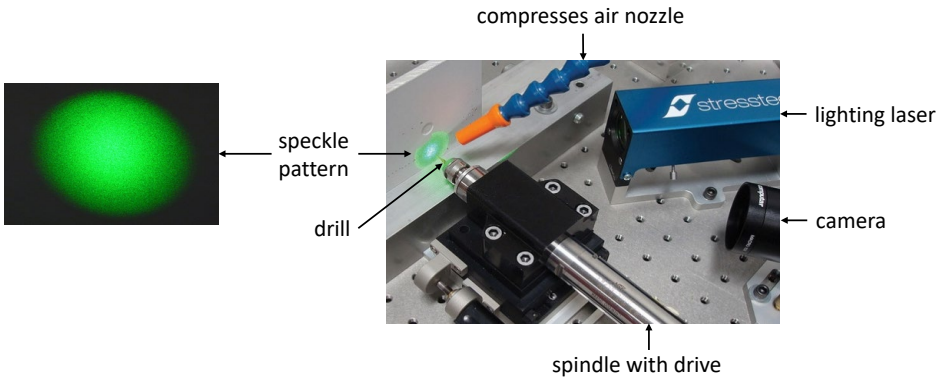

Fig. 2. ESPI setup

The reflected radiation is recorded with a CCD camera and reproduced as a black/white interference pattern, Figure 3. The blurred pattern is created because a single camera pixel intercepts reflected radiation from several locations on the irradiated surface and is displayed lighter or darker depending on the total intensity intercepted. Changes in this pattern after the ablation of a depth increment indicate deformations of the surface, which are used to calculate the stress state [23; 24].

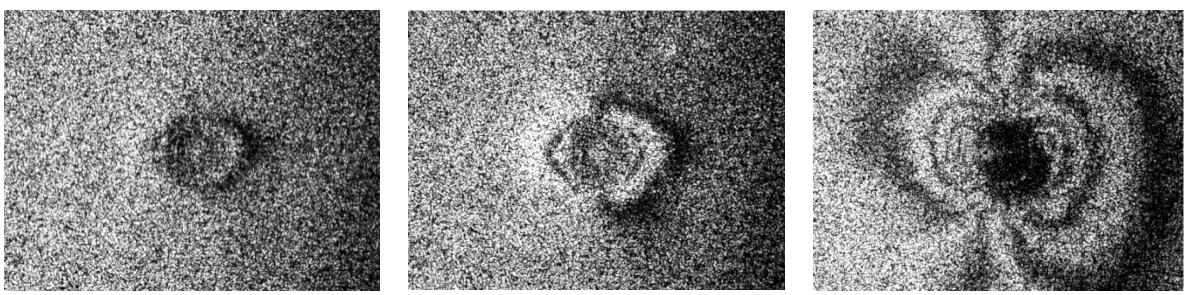

hole depth 0,01 mm | hole depth 0,05 mm | hole depth 0,15 mm

Fig. 3. Speckle pattern at different hole depths in the investigated material M280-30AP

The differential method according to Kockelmann [28] and the integral method according to Schajer [29] are widely used to calculate residual stresses from the measured data. In the differential method, it is assumed that only the last depth increment drilled leads to deformations, whereas the integral method takes into account the influence of all previously drilled depth increments on the deformation [24; 30]. The measurements carried out in this work were evaluated using the integral method.

The combination of the borehole method and ESPI allows quantification of microstresses at the sample surface in coarse-grained materials by drilling increments smaller than the average grain size. However, the stress state in the depth direction can only be mapped qualitatively. The penetration depth of the drill holes is usually about 60% of the drill diameter, as no further significant deformations are induced at the surface at

greater depths [31-33]. The results of this comparatively fast measurement method are comparable in their informative value to the more precise, but significantly more time- and cost-intensive residual stress measurement with X-ray diffraction (XRD), which is also well established [34; 35].

2. Experimental Setup

The material investigated is a non-grain-oriented, highly permeable electrical sheet M280-30AP (according to DIN EN 10027-1 and DIN 10106) with a nominal thickness of 0.30 mm. To reduce eddy current losses and for corrosion protection, the material is provided with an organic insulation layer which, due to these properties, cannot be removed for the joining process but should remain on the sheets as undamaged as possible. According to DIN EN 10342, the insulation coating is to be classified in the "EC-3" category of organic coatings. The EC-3 category is suitable for operating temperatures up to 180°C and can influence the weld penetration of the electrical sheet lamellae [36]. Possible undesired effects are defects such as spatter and pores as well as severe grain refinement and solidification.

A multimode disk laser (manufacturer: TRUMPF; model: "TruDisc 16002") with a wavelength of 1030 nm was used to perform the welds. The minimum beam power is 320 W at a maximum pulse frequency of 1000 Hz. The spot welds were produced with a beam power P_P = 400 W and a pulse duration of t_P = 56 ms, which results in a pulse energy of E_P = 22,5 J. At surface focus the effective beam diameter was measured to $d_{\sigma,eff}$ = 390 µm.

For each ESPI measurement, a blind hole with a diameter of 0.8 mm was drilled centrally in a spot weld. The measuring system used (manufacturer: Stresstech; model: "Prism") records a measuring range after each drilled depth increment, the diameter of which corresponds to four times the drill hole diameter. The measured values are given in the unit megapascal [MPa] for two measuring planes X and Y, which are arranged perpendicular to each other. Tensile stresses have a positive sign and compressive stresses have a negative sign.

For the investigations in this paper, drill holes with a total depth of 0.3 mm were drilled in depth increments of 0.01 mm each at a feed rate of 0.01 mm/s and a speed of 17000 rpm centrically in the spot welds produced. The frequency of faulty measurements increases significantly from a measurement depth of 0.15 mm. Therefore, only the first 15 depth increments are evaluated for the evaluation of the residual stress measurements.

3. Results

To assess the welding residual stresses caused by the joining process, the residual stresses present in the base metal due to the fabrication and shaping process were determined using the ESPI-assisted hole drilling method. Figure 4 shows the results of five reference measurements separately for both measurement planes (X-axis and Y-axis). All reference measurements are predominantly in a range from -500 MPa (compression) to +500 MPa (tension), occasionally up to approx. +900 MPa, whereby the tensile residual stresses predominate in the X-axis.

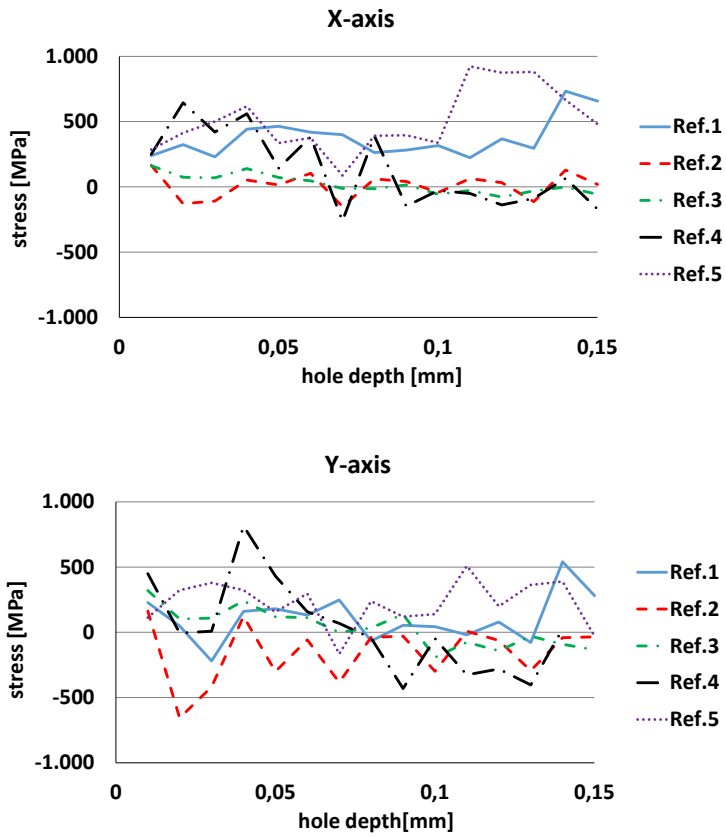

Fig. 4. Reference measurements of residual stresses in the base material; top: X-axis; bottom: Y-axis

When comparing these measurement results with the tensile strength of the material M280-30AP, which was determined to 530 MPa, it is noticeable that the residual stresses already partially exceed the tensile strength. The pronounced brittleness of the material expected from this does not occur. Furthermore, it has to be concerned, that the determination of residual stresses is not possible by direct measurement, but only indirectly and purely qualitatively. Therefore, the direct quantitative comparison of the tensile strength with the determined stresses is not permissible. However, the reference measurements have a high consistency and reproducibility, which is why they are used as a basis for classifying the residual stress measurements presented in the following.

The influence of the working pressure on the formation of welding residual stresses was investigated in surface focus, Figure 5. Tensile stresses were determined in the weld at all examined working pressures from p = 1 mbar to p = 1000 mbar. The similar courses of the measured values in the X and Y directions indicate a rotationally symmetrical stress distribution, which is to be expected for a single spot weld.

Within the first eight depth increments, i.e. a hole depth of 0.08 mm, comparable values in the range of up to 2000 MPa occurred for all working pressures investigated. At low working pressures of $p < 10$ mbar, this stress level remains constant up to the maximum measurement depth of 0.15 mm, whereas at higher working pressures $p > 100$ mbar, over 4000 MPa are reached.

A possible cause for the higher stress values is the pressure-dependent evaporation temperature of the material [37; 38]. At pressures > 100 mbar, the melt reaches higher temperatures than at $p < 100$ mbar

before the material evaporates. This increases the temperature gradient to the surrounding material, which increases the cooling rate of the melt and thus the expression of stresses. The melt contaminated by the carbon-containing insulation coating hardens during this rapid cooling [39; 40] and is less able to relieve stresses by deformation. Increased stress levels remain, which are up to a factor of eight higher than in the base material.

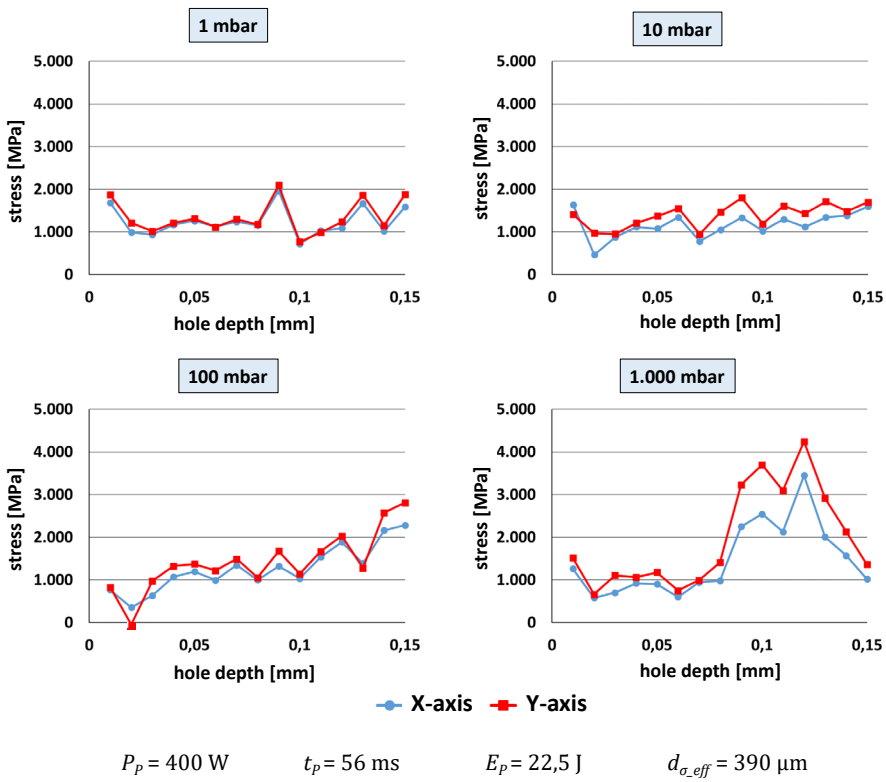

Fig. 5. ESPI stress measurements at different working pressures at surface focus

To investigate the influence of the beam intensity on the welding residual stresses, welding tests were carried out with focal positions from +1 mm ($d_{\sigma,eff}$ = 410 µm) to +4 mm ($d_{\sigma,eff}$ = 525 µm) at p = 1 mbar and p = 10 (Figure 6).

Comparable tensile stresses occur in both measuring planes X and Y. These are in a range of values up to approx. 2800 MPa, independent of working pressure and beam diameter.

At p = 10 mbar, the residual stresses increase slightly with all examined focal positions with increasing borehole depth but are in a similar range of values as for the welds in surface focus (Figure 5, top right).

The comparison to the surface focus shows no significant deviation as well at p = 1 mbar. However, it is noticeable that at p = 1 mbar the residual stresses at a beam diameter of $d_{\sigma,eff}$ = 525 µm are less pronounced over the entire measurement depth than at $d_{\sigma,eff}$ = 440 µm. Here, the combination of a reduction of the working pressure and the beam intensity seems to reduce the temperature gradient between the melt and the base material in such a way that the resulting residual stresses are also reduced.

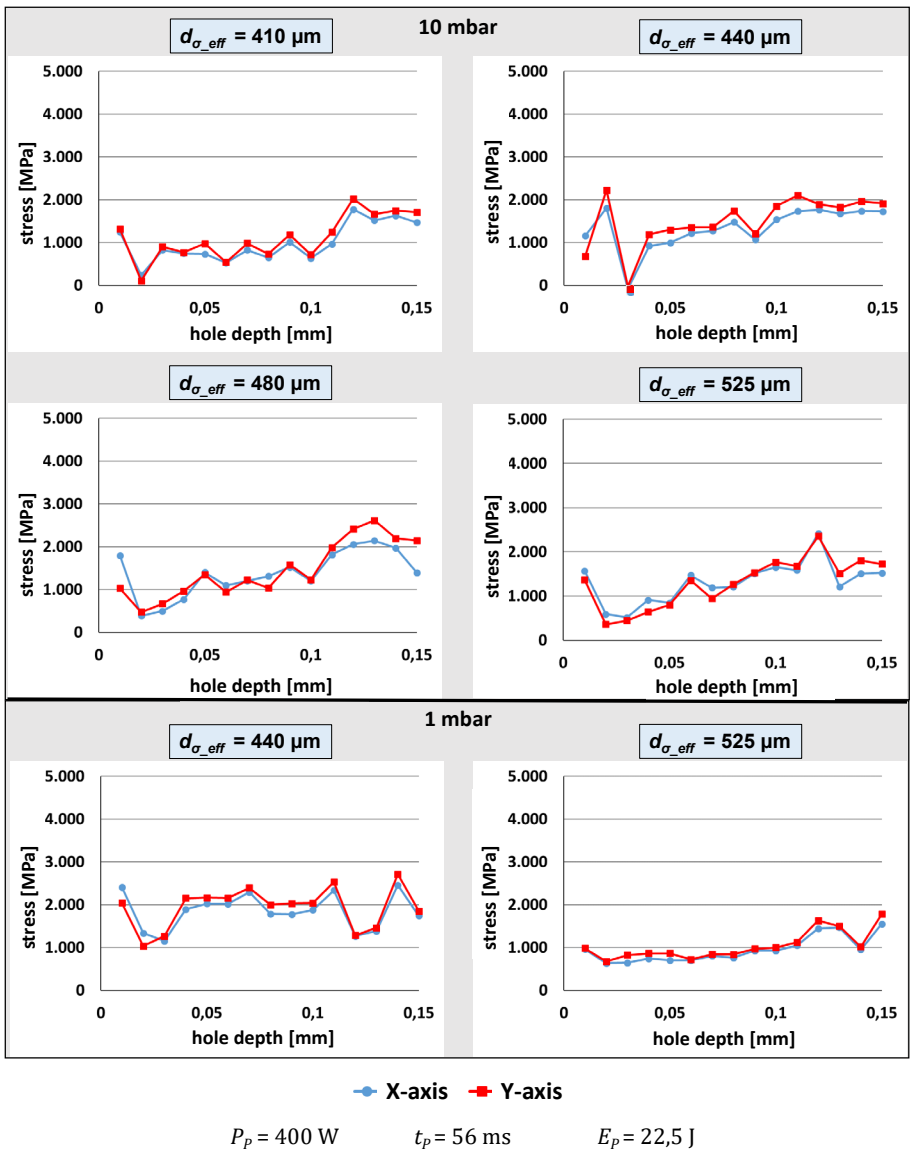

Fig. 6. ESPI stress measurements at different working pressures and beam diameters

4. Conclusions

To investigate the influence of beam intensity on the residual welding stresses, welding tests were carried out with beam diameters of $d_{\sigma,eff}$ = 390 µm to $d_{\sigma,eff}$ = 525 µm at working pressures of p = 1 mbar up to p = 1000 mbar.

Comparable tensile stresses occur in both measurement planes X and Y. These are independent of working pressure and welding pressure. These are in a range of values up to approx. 2800 MPa, independent of working pressure and focus position.

At p = 10 mbar, the residual stresses increase slightly with all examined focal positions with increasing borehole depth, but are in a similar value range as for the welds in the surface focus.

The comparison to the surface focus shows no significant deviation even at p = 1 mbar. However, it is noticeable that at p = 1 mbar the residual stresses at a bigger beam diameter are less pronounced over the entire measurement depth than at smaller beam diameters respectively higher intensities. The combination of a reduction of the working pressure as well as the beam intensity seems to reduce the temperature gradient between melt and base material in such a way that the resulting welding residual stresses are also reduced.

Acknowledgements

The presented investigations were carried out at RWTH Aachen University and funded by the Deutsche Forschungsgemeinschaft e.V. (DFG, German Research Foundation). The sponsorship and support is gratefully acknowledged.

References

[1] Burress, T. A. (2012): Benchmarking of Competitive Technologies. Oak Ridge National Laboratory, Washington, D.C.

[2] Burress, T. A. et al. (2008): Evaluation of the 2007 Toyota Camry Hybrid Synergy Drive System. DOI: 10.2172/928684.

[3] van Basshuysen, R. und F. Schäfer (2017): Handbuch Verbrennungsmotor. Wiesbaden: Springer Fachmedien Wiesbaden. ISBN: 978-3-658-10901-1. DOI: 10.1007/978-3-658-10902-8.

[4] Merker, G. P. und R. Teichmann (2019): Grundlagen Verbrennungsmotoren. Wiesbaden: Springer Fachmedien Wiesbaden. ISBN: 978-3-658-23556-7. DOI: 10.1007/978-3-658-23557-4.

[5] Matthies, G., K. Stricker und J. Traenckner (2010): The e-mobility era: Winning therace for electric cars. Bain & Company.

[6] Kampker, A. (2014): Elektromobilproduktion. Springer-Verlag. DOI: 10.1007/978-3-642-42022-1.

[7] Schneider, M., N. Urban und J. Franke (2017): Relation of joining parameters of stator core production and iron loss. DOI: 10.1109/EDPC.2017.8328148.

[8] Kurosaki, Y. e. a. (2008): Importance of punching and workability in non-oriented electrical steel sheets. In: *Journal of Magnetism and Magnetic Materials* 320 (20), pp. 2474–2480. DOI: 10.1016/j.jmmm.2008.04.073.

[9] Krings, A. e. a. (2017): Soft Magnetic Material Status and Trends in Electric Machines. In: *IEEE TRANSACTIONS ON INDUSTRIAL ELECTRONICS, Vol. 64, No. 3*, pp. 2405–2414. DOI: 10.1109/TIE.2016.2613844.

[10] Brachthäuser, N. (2012): Elektromobilität–Neue Herausforderungen an den Werkstoff Elektroband. TU Darmstadt, 07.03.2012.

[11] Lamprecht, E., M. Hömme und T. Albrecht (2012): Investigations of eddy current losses in laminated cores due to the impact of various stacking processes. In: *2nd International Electric Drives Production Conference (EDPC)*, pp. 1–8. DOI: 10.1109/EDPC.2012.6425097.

[12] Wang, H., Y. Zhang und S. Li (2016): Laser welding of laminated electrical steels. In: *Journal of Materials Processing Technology* (vol. 230), pp. 99–108. DOI: 10.1016/j.jmatprotec.2015.11.018.

[13] Schade, T. e. a. (2014): Electrical steel stacks for traction motors - fundamental investigation of the weldability. In: *Shaping the Future by Engineering: Proceedings; 58th IWK, Ilmenau Scientific Colloquium, Vol. 58*.

[14] Schoppa, A. P. et al. (2003): Influence of welding and sticking of laminations on the magnetic properties of non-oriented electrical steels. In: *J. Magn. Magn. Mater.*, 367-369. DOI: 10.1016/S0304-8853(02)00877-6.

[15] Clerc, A. J. und A. Muetze (2012): Measurement of Stator Core Magnetic Degradation During the Manufacturing Process. In: *IEEE TRANSACTIONS ON INDUSTRY APPLICATIONS, Vol. 48, No. 4*, 1344-1352. DOI: 10.1109/TIA.2012.2199950.

[16] Vourna, P. (2014): Characterization of Electron Beam Welded Non-Oriented Electrical Steel with Magnetic Barkhausen Noise. In: *Key Engineering Materials* (vol. 605), pp. 39–42. DOI: 10.4028/www.scientific.net/KEM.605.39.

[17] Radaj, D. (2002): Eigenspannungen und Verzug beim Schweißen: Rechen- und Messverfahren, DVS-Verlag, Fachbuchreiche Schweißtechnik (Bd. 143), ISBN 3-87155-194-5.

[18] Schoppa, A. P., J. Schneider und C.-D. Wuppermann (2000): Influence of the manufacturing process on the magnetic properties of non-oriented electrical steels. In: *Journal of Magnetism and Magnetic Materials* 215-216, pp. 74–78. DOI: 10.1016/S0304-8853(00)00070-6.

[19] Schoppa, A. P., J. Schneider und J.-O. Roth (2000): Influence of the cutting process on the magnetic properties of non-oriented

electrical steels. In: *J. Magn. Magn. Mater.* (Vol. 215/216), pp. 100–102. DOI: 10.1016/S0304-8853(00)00077-9.

[20] Tölle, F. (2013): Eigenspannungsreduktion in strahlgeschweißten Nähten mittels Spannungsumlagerung durch den Einsatz defokussierter Elektronen- bzw. Laserstrahlen [Dissertation]. BAM-Dissertationsreihe Band 105. Berlin.

[21] ASTM E837-08 (2008): Standard Test Method for Determining Residual Stresses by the Hole-Drilling Strain- Gage Method.

[22] Held, E. (2014): Eigenspannungsanalyse an Schichtverbunden mittels inkrementeller Bohrlochmethode [Dissertation]. Karlsruhe: KIT Scientific Publishing. ISBN 3731501279.

[23] Rendler, N. J. und Vigness, I. (1966): Hole-drilling strain-gage method of measuring residual stresses. In: *Experimental Mechanics* 6 (12), pp. 577–586. DOI: 10.1007/BF02326825.

[24] Schajer, G. S. und Steinzig, M. (2005): Full-field calculation of hole drilling residual stresses from electronic speckle pattern interferometry data. In: *Experimental Mechanics* 45 (6), pp. 526–532. DOI: 10.1007/BF02427906.

[25] Mathar, J. (1933): Determination of Initial Stresses by Measuring the Deformation Around Drilled holes. In: *Transactions of the ASME, Iron & Steel, Vol. 56*, pp. 249–254.

[26] Genzel, C., I. A. Denks und M. Klaus (2013): Modern diffraction methods - Residual Stress Analysis by X-Ray Diffraction Methods. John Wiley & Sons, ISBN: 978-3-527-32279-4.

[27] Wolfstieg, U. und E. Macherauch (1973): Ursachen und Bewertung von Eigenspannungen. In: *Chemie Ingenieur Technik*, pp. 760–770. DOI: 10.1002/cite.330451103.

[28] Schwarz, T. und H. Kockelmann (1993): Die Bohrlochmethode – ein für viele Anwendungsbereiche optimales Verfahren zur experimentellen Ermittlung von Eigenspannungen. In: *Messtechnische Briefe 29.2*, pp. 33–38.

[29] Schajer, G. S. (1988): Measurement of Non-Uniform Residual Stresses Using the Hole- Drilling Method. Part I—Stress Calculation Procedures. In: *Journal of Engineering Materials and Technology Vol. 110*, pp. 338–343.

[30] Schajer, G. S. (1981): Application of Finite Element Calculations to Residual Stress Measurements. In: *Journal of Engineering Materials and Technology* 103 (2), pp. 157–163. DOI: 10.1115/1.3224988.

[31] Grant, P.V., J.D. Lord und P.S. Whitehead (2006): The Measurement of Residual Stresses by the Incremental Hole Drilling Technique. In: *Measurement Good Practice Guide No. 53 Issue 2*.

[32] Tech Note TN-503-6 (2010): Measurement of Residual Stresses by the Hole-Drilling Strain Gage Method. Vishay Micro-Measurements.

[33] Bobzin, K. e. a. (2020): Comparison of Residual Stress Measurements Conducted by X-ray Stress Analysis and Incremental Hole Drilling Method. In: *J Therm Spray Tech*. DOI: 10.1007/s11666-020-01056-z.

[34] Rickert, T. J. et al. (2014): Residual Stress Measurement of Shot-Peened Steel Rings by Barkhausen Noise, ESPI Hole-Drilling and X-Ray Diffraction. In: *Advanced Materials Research* 996, pp. 380–385. DOI: 10.4028/www.scientific.net/AMR.996.380.

[35] Reisgen, U. e. a. (2017): Residual stress measurement in AlSi alloys. In: *Materialwissenschaft und Werkstofftechnik*, pp. 1270–1275. DOI: 10.1002/mawe.201700157.

[36] DIN EN 10342 (2005): Magnetische Werkstoffe - Einteilung der Isolationen auf Elektroblech. Beuth Verlag, Berlin.

[37] Honig, R. E. und D. A. Kramer (1969): Vapor Pressure data for the solid and liquid elements. In: *Radio Corporation of America (RCA) Review, Vol. 30*, pp. 285–305.

[38] Zhang, Y., J. R. G. Evans und S. Yang (2011): Corrected Values for Boiling Points and Enthalpies of Vaporization of Elements in Handbooks. In: *Journal of Chemical & Engineering Data, 56*, pp. 328–337. DOI: 10.1021/je1011086.

[39] Krichel, T., Olschok, S., Reisgen, U. (2022): Influence of working pressure on laser beam welding in vacuum of electrical steel sheets. In: *Vacuum*, p. 111659. DOI: 10.1016/j.vacuum.2022.111659.

[40] Krichel, T. (2021): Laser in Vacuum spot welding of electrical steel sheets with 3.7 % Si-content. In: *Lasers in Manufacturing (LiM); Online-Konferenz, 21.06.2021*.